The Ascension Island experiment

Belcher, David; Cannon, P.S.; Gustavsson, Anders

DOI:
10.1109/IGARSS.2015.7326496

License:
Other (please specify with Rights Statement)

Document Version
Peer reviewed version

Citation for published version (Harvard):
Belcher, D, Cannon, PS & Gustavsson, A 2015, The Ascension Island experiment: measurement of ionospheric scintillation effects on PALSAR-2. in *2015 IEEE International Geoscience and Remote Sensing Symposium (IGARSS)*. IEEE International Geoscience and Remote Sensing Symposium proceedings, Institute of Electrical and Electronics Engineers (IEEE), pp. 3191-3194, International Geoscience and Remote Sensing Symposium 2015 (IGARSS 2015), Milan, Italy, 26/07/15. https://doi.org/10.1109/IGARSS.2015.7326496

THE ASCENSION ISLAND EXPERIMENT: MEASUREMENT OF IONOSPHERIC SCINTILLATION EFFECTS ON PALSAR-2

D. P. Belcher[1], *P. S. Cannon*[1] *and A. Gustavsson*[2]
[1] University of Birmingham, UK.
[2] Swedish Defence Research Agency (FOI), Linköping, Sweden.

ABSTRACT

The effect of the ionosphere on SAR imaging has been studied previously from both an analytic and a numerical simulation perspective. Recently, effects visible in SAR imagery have been ascribed to turbulence in the ionosphere. This paper describes an experiment that seeks to use ground-based GPS measurements of the ionospheric scintillation, collected simultaneously with PALSAR-2 imagery, to unambiguously confirm the predictions of the analytic theory. PALSAR-2 (on board the ALOS-2 satellite) was used in spotlight mode to image a 5m corner reflector to obtain an accurate measurement of the point spread function (PSF). Initial results, obtained during the 2014/15 scintillation season, confirm that the analytic theory describing the shape of the SAR PSF is correct. This is then used to obtain two measures of the scintillation, p and C_kL, directly from the PALSAR-2 PSF. The collected data set can also be used for further research into ionospheric autofocus techniques.

***Index Terms*—**Synthetic Aperture Radar, Ionosphere, Ionospheric Scintillation

1. INTRODUCTION

An important application of space-based synthetic aperture radar (SAR) is the global monitoring and measurement of terrestrial biomass, accurate figures for which are required for global climate change calculations. Most SARs use high frequencies (C-band or above) in which case the backscattered radar signal largely comes from the top few centimeters of vegetation and the radar is consequently unable to measure the full extent of the biomass. This drives the radar designer to use lower frequencies, ideally P-band (UHF) or below, so that penetration through dense forest stands is achieved and the total biomass is accurately measured.

At these lower frequencies, the space-based radar signal is affected by propagation through small-scale ionospheric turbulence [1] which is prevalent in the equatorial and high latitude regions. The ionospheric turbulence represents an important limiting factor [2] in the operation of these radars and has been explored through numerical simulations, but these are computer intensive, time consuming and provide little insight. Computationally inexpensive analytic approaches offer many advantages but until recently they have not been explored. In [3] and [4] the effect of the ionosphere on the SAR image point spread function (PSF) was analytically predicted using the C_kL statistical description of ionospheric turbulence [5]. These analytic predictions were compared with a validated numerical propagation model [6, 7] and the agreement has been shown to be good [4]. Although numerical simulations represent an important part of the validation (and a full diffraction accurate simulation was used) a simulation will inevitably make some assumptions about the real and highly complex ionosphere. Clearly, if these assumptions are the same as those made in the analytic approach, the simulation cannot be regarded as a proper test of that approach. An experimental validation of the analytic theory is thus required.

The effects of the ionosphere's bulk total electron content (TEC) have been detected on experimental data via the Faraday rotation [8] and via its effect on interferometry [9]. The ionospheric turbulence manifests itself as scintillation (the random fluctuations of phase and amplitude) of any electromagnetic wave passing through it. Defocusing effects seen in the SAR imagery have therefore also been ascribed to the ionosphere [10]. However, there are few well instrumented examples of the impact of the ionosphere's turbulence on space-based SAR. For the effects on a SAR image to be shown to be due to the turbulent ionospheric irregularities, both independent measurements of the state of the ionosphere and SAR imaging are required simultaneously.

This paper describes a novel experiment that obtained PALSAR-2 images through a turbulent equatorial ionosphere which was simultaneously measured using global positioning service (GPS) receivers. This both unambiguously establishes that the effects on the SAR point spread function (PSF) are due to the ionosphere (and not some other effect such as target motion) and confirms the analytic theory predicting the shape of the PSF. The inverse problem (that of determining the ionospheric state from the PSF) can then also be solved.

2. EXPERIMENTAL CONFIGURATION

2.1 Experiment design

The impact of ionospheric scintillation on SARs is difficult to observe because the lowest operational frequency is currently at L-band. The onset of scintillation is also only probabilistically predictable from climatological models such as WBMOD [11]. The experiment therefore needs to collect as many SAR images as possible in an area where the probability of significant ionospheric turbulence, and hence scintillation is high.

The site was selected using the WBMOD model which provides global estimates of the strength of ionospheric scintillation, as described by the strength of turbulence parameter, C_kL. Ascension Island (14ºW 8ºS), located on the mid Atlantic ridge, just south of the equator, in a region of anomalously high scintillation known as the equatorial anomaly, was selected. This scintillation is particularly pronounced during Ascension's scintillation season (September to March inclusive) and near the peak of the sun-spot cycle.

Ascension Island also has the appropriate infrastructure for the installation and continuous operation of GPS L-band scintillation receivers. These provide independent measurements of the ionospheric turbulence parameter C_kL and spectral slope p which are input parameters to the analytic model of the PSF [4].

One of the most obvious effects of scintillation on SAR imagery is to raise the sidelobes of point (corner reflector) targets, and this sidelobe level in dB is predicted [3, 4] to be directly proportional to the level of log C_kL. However, at L-band, the effects of scintillation are slight, so the experiment needs to use high RCS corner reflectors, preferably placed on a low RCS background, to perform this measurement. The corner reflectors chosen were originally used to calibrate PALSAR imagery [12] and are of side length 5m, giving an RCS of approximately 47dBm^2. An important advantage of near equatorial imaging is that the corner reflectors can be fixed in position and do not need to be adjusted for each satellite pass.

2.2 The PALSAR-2 radar

PALSAR-2 is an L-band space-based SAR that can produce single look complex imagery at a resolution of up to 1m in the spotlight mode. The main characteristics of PALSAR-2 are shown in Table 1 [13, 14]. PALSAR-2 was chosen for this experiment for a number of reasons. Firstly, the ionospheric effects are most visible at lower frequencies, and L-band is the lowest currently available. Secondly, the effects of scintillation are most visible in the along track direction at the highest resolutions, and 1m is the highest available. Thirdly, PALSAR-2 is in near polar orbit, so the azimuth angle of a corner reflector target placed near the equator does not need to be changed for each satellite pass. Finally, the ionospheric scintillation events are most severe in the early evening after sunset. PALSAR-2 imaging on the ascending node with its equatorial crossing at 00:00 local time, and preferably looking west into the sunset, provides good opportunities for this. The sun-spot cycle will also be near its maximum in 2014, thus resulting in a much larger chance of scintillation.

Although PALSAR-2 is normally operated at only one incidence angle to ensure consistency of coverage, the instrument itself is actually capable of performing SAR imaging at a wide variety of incidence angles. Since the experiment would benefit from as much data as possible, the experiment has also been designed to work at all the incidence angles at which PALSAR-2 can operate. As the range from the reflector to PALSAR-2 increases with increasing incidence angle, the signal to noise ratio in the SAR image decreases, but so too does the clutter. Since PALSAR-2 is generally clutter, rather than noise, limited at least when using 5m corner reflector targets, imagery at all incidence angles can be fully utilized in this experiment. Optimising the corner reflector incidence angle for 45° rather than the smaller incidence angles increases the signal to noise ratio at shallower grazing angles and longer ranges.

Ascension Island itself is fully contained within one standard 25 km x 25 km scene, so there are no issues of contention with other users or of ensuring that contiguous imagery has the same incidence angle. PALSAR-2 can be right or left looking, but ionospheric effects will be maximized for a left looking SAR on the ascending node since this looks into the sunset.

The incidence angle of PALSAR-2 can be between 8° and 70°. The incidence angle is greater than the off-nadir antenna elevation pointing angle by the longitude subtended at the equator between the satellite and the target. The spotlight mode uses only a single polarization due to PRF and data rate considerations, but the effect of scintillation on the Faraday rotation is slight compared to the constant bulk TEC slab effects.

Table 1 PALSAR-2 radar parameters

Centre frequency	1257.5 MHz		
PRF	1 – 6 kHz		
Antenna length	10.0 m x 3.0 m (az x el)		
Transmit power	6.1 kW		
Look direction	Left or Right (optional)		
Maximum range	1160 km		
Radar modes	**Spotlight**	**Strip-map Ultra-fine**	**Strip-map High**
Resolution (along track)	1 m	3 m	6 m
Range transmit bandwidth	84 MHz	84 MHz	42 MHz
Range receive sampling	105 MHz	105 MHz	52 MHz
Slant range resolution	3 m	3 m	6 m
Polarization	SP	SP/DP	SP/DP/ FP/CP
Incidence angles	8-70°	8-70°	8-70°
Swath size	25 x 25 km	50 km	50 km (30km FP)
NESZ (σ_{0NE})	-24 dB	-24 dB	-28 dB

2.3 The ALOS-2 satellite

The ALOS-2 satellite which carries PALSAR-2 is in a sun synchronous orbit with a 14 day repeat cycle, during which time it orbits the Earth 207 times. In consequence it has 207 ground tracks, which are numbered from #1 to #207, the orbital geometry to a fixed ground point being identical for the same track number, regardless of the orbit cycle number. PALSAR-2 imaging during the midnight pass (ascending node) rather than the midday pass increases the probability of scintillation, despite the TEC being higher during the day. The orbital parameters are shown in Table 2.

Table 2 ALOS2 orbit characteristics

Altitude (above mean equatorial radius)	628 km
Inclination angle	97.92°
Orbital time period	97.39 minutes
Local time of equator crossing	00:00 (ascending)
Repeat cycle	14 days, 207 orbits
Longitude offset of track #1	25.815° W
Orbit Duty Cycle	50%

2.4 Orbit considerations

The above orbital information can be combined with the radar parameters to determine, at least approximately, the visibility of the target from the satellite. Using the spherical cosine rule, and the ground track numbering scheme, the target corner reflector's broadside bearing, (and hence RCS change with angle), slant/ground range, incidence and grazing angle can all be

determined, some of which are shown in Table 3. The main conclusions are as follows:

- The range to the target from the satellite generally increases with the track number, the increasing range also raising the noise equivalent σ_0 (i.e. σ_{0NE}). Although the σ_{0NE} is very good at close range, the incidence angles are so small that the reflection from the clutter dominates, thus making low level sidelobes less visible. Very steep grazing angles are therefore not particularly useful for measuring this effect, whereas shallow ones have high noise levels.
- The bearing angle to the satellite from the target reflector decreases slightly as the range increases. This is because for a right looking geometry, the target is being imaged from a point further away, and thus further south on the sinusoidal ground track. However, the angular change is less than ±1°, thus justifying the fixing of the corner reflector.
- The orbital altitude of PALSAR-2 is 628km, which is approximately twice that of the ionosphere at 350km, so the ionospheric penetration point (IPP) is approximately half way between the satellite and the ground target. Ascension Island is only just south of the equator, so when imaging the target, the satellite is only 2 or 3 minutes from its equator crossing, and so the local time of the satellite is nearly identical for all tracks. Since the IPP is approximately half way between the satellite and target, the local time at the IPP is half way between the satellite local time and the target local time, which is GMT plus 57 minutes. The local time at the IPP is generally about half an hour before or after midnight, depending on whether it is right or left looking.

Table 3 Track imaging geometry for corner reflector (CR) target

Track #	Slant range (km)	Incidence at IPP θ°	CR bearing to satellite (°N))	CR grazing angle (°)
204	740.3	30.9	261.2	57.2
205	859.7	42.1	260.9	45.0
206	1004.9	50.4	260.5	35.7
207	1165.1	56.3	260.1	28.7
1	1335.8	60.6	259.7	23.2
2	1512.1	63.9	259.2	18.8

The IPP moves along the ionosphere as the synthetic aperture is formed; Fig 1 shows the section along the ionosphere when imaging the corner reflector for each track.

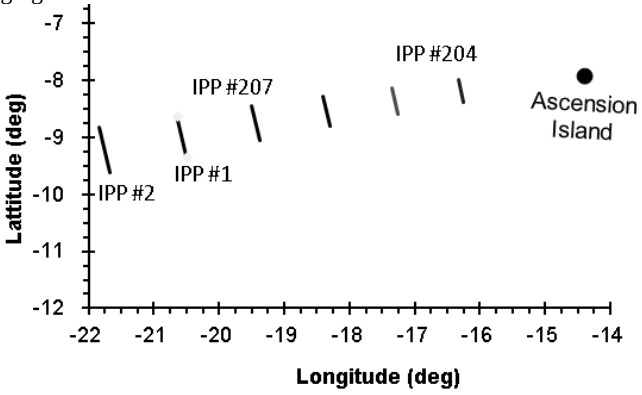

Fig 1 The location of the IPP (right looking only)

The effective velocity ratio γ and anisotropic geometric enhancement factor G can be determined for the IPP tracks in Fig 1 using the method of [15]. When combined with the outer scale l_0, the effective outer scale along the synthetic aperture is $\gamma l_0 \approx 30$ km and $G \approx \sec\theta$ where θ is the incidence angle at the IPP.

2.5 GPS receivers

An important aspect of the experiment is to be able to compare PALSAR-2 images with simultaneous independent measurements of the ionospheric turbulence. These measurements are provided by the use of carrier phase tracking GPS receivers with a Rubidium clock. The GPS receivers used are GSV 4004 and are primarily used to measure the phase power spectrum of the ionospheric disturbance.

Ideally, the GPS signal should be received through exactly the same part of the ionosphere, and simultaneously with, that through which the SAR signal passes. The GPS constellation consists of 24 satellites in 6 planes, at an altitude of 22 000km. Since the inclination is 55°, an exact match with PALSAR-2 (98°) is impossible, but the correlations that are likely to be experienced in the ionosphere should enable an independent estimate of the scintillation strength and the spectral slope p to be made.

3. RESULTS

3.1 Corner reflector location

Two corner reflectors (CRs) have been placed on Ascension Island, one looking East, located on the East side of the island, and one looking West, located on the West side of the island. Their base was placed flat and level, and was secured firmly in place, their side length being 5.15 m. Their precise positions were measured by a dual frequency GPS receiver and are shown in Table 4.

Table 4 Location of Corner Reflectors

	EAST CR	WEST CR
Location name	Devils Ashpit	Long Beach
Boresight bearing (azimuth, deg true N)	80°	260°
Boresight elevation (deg)	45°	45°
Latitude (deg)	-7. 9542 1890	-7. 9142 5420
Longitude (deg)	-14. 3262 0501	-14. 4020 3588
Altitude (m)	548.32	42.06
Location accuracy	Position ~ 10cm; angles 1°	
Co-ordinate system	WGS-84	

3.2 The point spread function (PSF)

Under ionospheric disturbance, the SAR point spread function is equal to the mainlobe plus sidelobes, the ensemble average sidelobe shape being given by [4, 16]

$$\langle|\eta(r)|^2\rangle = T_{SLF}\left(\sqrt{r_0^2 + r^2}\right)^{-p} \approx T_{SLF} r^{-p}$$

where T_{SLF} is the turbulence of the sidelobes, p is the ionospheric phase screen spectral index, $r_0 = L_{SA}/\gamma l_0$, which is approximately 3 for this data, and r is the along track resolution cell, the centre of the mainlobe being cell 1, the first sidelobe cell 2, etc. The approximate form is valid when $r \gg r_0$.

The PSF is an even function, so right and left sidelobes can be averaged, and displaying on a log-log plot should therefore result in a straight line of slope p and intercept T_{SLF} dB. Fig 2 shows the

PSF of the West CR on 18 Aug 2014, which is before the start of the scintillation season. The PSF is very narrow, achieving a 3dB resolution of 1m, and a 35dB width of less than 10m. This is essentially the PSF in the absence of ionospheric effects, and consists largely of the mainlobe. This is confirmed by the measured GPS amplitude scintillation index $S_4 = 0.0$.

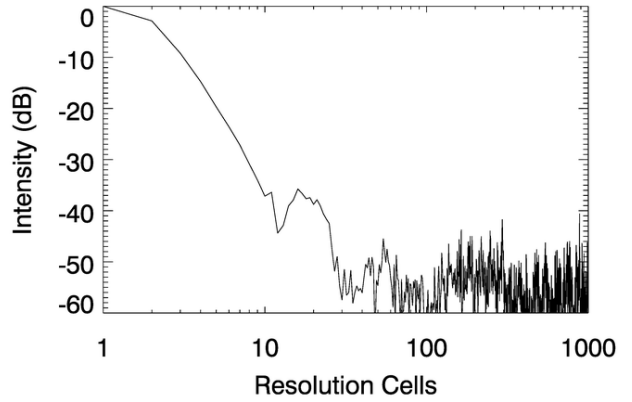

Fig 2 The spotlight PSF at 1m resolution (18 Aug 2014)

The same CR is shown in Fig 3 on 23 Nov 2014, during the scintillation season. The dotted line represents the fitted sidelobe shape, with $p = 2.03$ and $T_{SLF} = 7.76$ dB. Using the known relationship of T_{SLF} to $C_k L$ [4, 16] the value of $\log_{10}(\mathrm{C_k L}) \approx 33.9$ not unreasonable during the scintillation season near the peak of the sun-spot cycle. The measured GPS $S_4 = 0.3$ for this PSF, which is therefore unambiguously the result of scintillation.

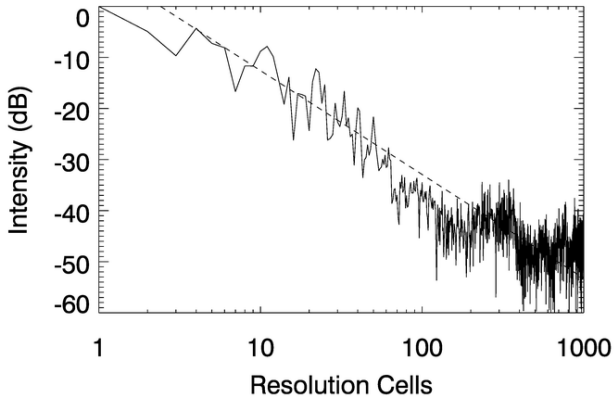

Fig 3 The spotlight PSF at 1m resolution (23 Nov 2014)

Initial results from the other PSFs suggest that, during the scintillation season, not only are the sidelobes raised, as in Fig 3, but defocusing often occurs. Thus the collected SAR data, together with the simultaneously collected GPS data set, represents an excellent resource for future research.

The full data from the GPS receivers will be retrieved from Ascension Island shortly.

ACKNOWLEDGEMENTS

The authors wish to thank JAXA Japan for the PALSAR-2 data, and Dr Shimada in particular; and also FOI, Sweden for the loan of the 5m corner reflectors.

REFERENCES

[1] D. P. Belcher, "Theoretical limits on SAR imposed by the ionosphere", *IET Radar, Sonar and Navigation,* vol. 2, pp. 435-448, 2008, doi:10.1049/iet-rsn:20070188.

[2] P. S. Cannon, *et al.*, "Signal distortion on VHF/UHF transionospheric paths: First results from Wideband Ionospheric Distortion Experiment", *Radio Science,* vol. 41, 2006, doi:10.1029/2005RS003369.

[3] D. P. Belcher, "Sidelobe prediction in transionospheric SAR imaging radar from the ionospheric turbulence strength CkL", in Radar 2008 Conf., Adelaide, Australia, 2008, doi:10.1109/RADAR.2008.4653891

[4] D. P. Belcher and N. C. Rogers, "Theory and simulation of ionospheric effects on synthetic aperture radar", *IET Radar, Sonar and Navigation,* vol. 3, pp. 541-551, 2009, doi:10.1049/iet-rsn.2008.0205.

[5] C. L. Rino, "A power law phase screen model for ionospheric scintillation 1. Weak scatter", *Radio Science,* vol. 14, pp. 1135-1145, 1979.

[6] N. C. Rogers, *et al.*, "Measurements and simulation of ionospheric scattering on VHF and UHF radar signals: Channel scattering function", *Radio Science,* vol. 44, 2009, doi:10.1029/2008RS004033.

[7] N. C. Rogers, *et al.*, "Measurements and simulation of ionospheric scattering on VHF and UHF radar signals: Coherence times, coherence bandwidths and S4", *Radio Science,* vol. 44, 2009, doi:10.1029/2008RS004035.

[8] J. Nicoll, *et al.*, "Prediction and detection of Faraday rotation in ALOS PALSAR data", in *IEEE Geoscience and Remote Sensing Symposium (IGARSS 2007)*, Barcelona, Spain, 2007, pp. 5210-5213, doi:10.1109/IGARSS.2007.4424036.

[9] A. L. Gray, *et al.*, "Influence of ionospheric electron density fluctuations on satellite radar interferometry", *Geophys. Res. Lett.,* vol. 27, pp. 1451-1454, 2000.

[10] B. Hsueh, *et al.*, "A study on smearing due to ionospheric phase scintillation in SAR data", *Int. J. Remote Sensing*, vol. 34, pp. 1823-1837, 2013.

[11] J. A. Secan, *et al.*, "An improved model of equatorial scintillation", *Radio Science,* vol. 30, pp. 607-617, 1995.

[12] L. E. B. Eriksson, *et al.*, "ALOS PALSAR calibration and validation results from Sweden", in *IEEE Geoscience and Remote Sensing Symposium (IGARSS 2007)*, Barcelona, Spain, 2007, pp. 1589-1592, doi:10.1109/IGARSS.2007.4423115.

[13] Y. Kankaku, *et al.*, "The overview of the L-band SAR onboard ALOS-2", in Progress in Electromagnetics Research Symposium (PIERS 2009), Moscow, Russia, 2009.

[14] Y. Kankaku, *et al.*, "ALOS-2 mission and development status", in *IEEE Geoscience and Remote Sensing Symposium (IGARSS 2013)*, Melbourne, Australia, 2013, pp. 2396-2399.

[15] D. P. Belcher and P. S. Cannon, "Amplitude scintillation effects on SAR", *IET Radar Sonar Navig.,* vol. 8, pp. 658-666 2014, doi:10.1049/iet-rsn.2013.0168.

[16] D. P. Belcher and P. S. Cannon, "Ionospheric effects on synthetic aperture radar (SAR) clutter statistics", *IET Radar Sonar Navig.,* vol. 7, pp. 1004-1011, 2013, doi:10.1049/iet-rsn.2012.0227.